Monthly Notices of the ROYAL ASTRONOMICAL SOCIETY

MNRAS **493,** 1277–1291 (2020)
Advance Access publication 2020 February 6

doi:10.1093/mnras/staa343

The infrared view of dust and molecules around V4334 Sgr (Sakurai's object): a 20-yr retrospective

A. Evans,[1★] R. D. Gehrz,[2] C. E. Woodward,[2] D. P. K. Banerjee,[3] T. R. Geballe,[4] G. C. Clayton,[5] P. J. Sarre,[6] S. Starrfield,[7] K. Hinkle,[8] R. R. Joyce,[8] Foteini Lykou,[9,10] L. A. Helton,[2,11] S. P. S. Eyres,[12,13] H. Worters,[14] E. J. Montiel,[11,15] T. Liimets,[16,17] A. Zijlstra,[9,18] M. Richter[15] and J. Krautter[19]

[1]*Astrophysics Group, Keele University, Keele, Staffordshire ST5 5BG, UK*
[2]*Minnesota Institute for Astrophysics, School of Physics & Astronomy, University of Minnesota, 116 Church Street SE, Minneapolis, MN 55455, USA*
[3]*Physical Research Laboratory, Ahmedabad 380009, Gujarat, India*
[4]*Gemini Observatory, 670 N. Aohoku Place, Hilo, HI 96720, USA*
[5]*Department of Physics and Astronomy, Louisiana State University, Baton Rouge, LA 70803, USA*
[6]*School of Chemistry, The University of Nottingham, University Park, Nottingham NG7 2RD, UK*
[7]*School of Earth and Space Exploration, Arizona State University, PO Box 871404, Tempe, AZ 85287-1404, USA*
[8]*NSF's National Optical-Infrared Astronomy Research Laboratory, PO Box 26732, Tucson, AZ 85726, USA*
[9]*Department of Physics, The University of Hong Kong, C.Y.M. Physics Building, Pokfulam Road, Hong Kong*
[10]*Laboratory for Astrophysics, The University of Hong Kong, 100 Cyberport Road, Cyberport, Hong Kong*
[11]*USRA-SOFIA Science Center, NASA Ames Research Center, Moffett Field, CA 94035, USA*
[12]*Faculty of Computing, Engineering and Science, University of South Wales, Treforest, Pontypridd CF37 1DL, UK*
[13]*Jeremiah Horrocks Institute, University of Central Lancashire, Preston, Lancashire PR1 2HE, UK*
[14]*South African Astronomical Observatory, PO Box 9, Observatory, Cape Town 7935, South Africa*
[15]*Department of Physics, University of California Davis, 1 Shields Ave, Davis, CA 95616, USA*
[16]*Tartu Observatory, University of Tartu, Observatooriumi 1, 61602 Tõravere, Estonia*
[17]*Astronomický ústav, Akademie věd České republiky, v.v.i., Fričova 298, CZ-251 65 Ondřejov, Czech Republic*
[18]*Jodrell Bank Centre for Astrophysics, School of Physics and Astronomy, University of Manchester, Oxford Road, Manchester M13 9PL, UK*
[19]*Landessternwarte-Zentrum für Astronomie der Universität, Königstuhl, D-69117 Heidelberg, Germany*

Accepted 2020 January 31. Received 2020 January 31; in original form 2019 June 14

ABSTRACT

We present an analysis of the evolution of circumstellar dust and molecules in the environment of the very late thermal pulse object V4334 Sgr (Sakurai's object) over an ∼20-yr period, drawing on ground-, airborne-, and space-based infrared photometry and spectroscopy. The dust emission, which started in 1997, resembles a blackbody that cooled from ∼1200 K in 1998 August to ∼180 K in 2016 July. The dust mass, assuming amorphous carbon, was $\sim 5 \times 10^{-10}\,M_\odot$ in 1998 August, and we estimate that the total dust mass was $\sim 2 \times 10^{-5}\,M_\odot$ by ∼2016. The appearance of a near-infrared excess in 2008 suggests that a new episode of (or renewed) mass-loss began then. We infer lower limits on the bolometric luminosity of the embedded star from that of the dust shell, which rose to $\sim 16\,000\,L_\odot$ before declining to $\sim 3000\,L_\odot$. There is evidence for weak 6–7 μm absorption, which we attribute to hydrogenated amorphous carbon formed in material ejected by Sakurai's object during a mass ejection phase that preceded the 1997 event. We detect small hydrocarbon and other molecules in the spectra, and trace the column densities in hydrogen cyanide (HCN) and acetylene (C_2H_2). We use the former to determine the $^{12}C/^{13}C$ ratio to be 6.4 ± 0.7, 14 times smaller than the Solar system value.

Key words: stars: AGB and post-AGB – stars: carbon – circumstellar matter – stars: evolution – stars: individual, V4334 Sgr (Sakurai's object) – infrared: stars.

★ E-mail: a.evans@keele.ac.uk

1 INTRODUCTION

It is well known that the fate of a star when it evolves away from the main sequence (MS) depends on its mass. The 'text-book' scenario (Iben & Renzini 1983) for the post-MS evolution of low- to intermediate-mass stars is that, following the helium core flash, the burnout of He occurs in the core on the horizontal branch. After evolution up the asymptotic giant branch (AGB), the star sheds its outer envelope, which is illuminated as a planetary nebula (PN) by the still-hot stellar core. In time, the PN disperses and its nucleus becomes a white dwarf (WD).

However, in as many as 10–20 per cent of cases (Blöcker 2001; Lawlor & MacDonald 2003) the star, even after it has taken the left turn at the 'knee' beyond the post-AGB phase on the Hertzsprung–Russell (HR) diagram and is evolving downwards towards the WD region, reignites a residual helium shell in a very late thermal pulse (VLTP). It then retraces a large part of its evolutionary track (Iben 1982; Herwig 2001; Lawlor & MacDonald 2003) and becomes a 'born-again giant' (BAG). A number of examples of the VLTP phenomenon are now known, including Sakurai's object (V4334 Sgr; hereafter 'Sakurai') and V605 Aql. FG Sge has also been regarded as a BAG (Gehrz et al. 2005), although it is also regarded as a late thermal pulse (Jeffery & Schönberner 2006). All these stars are hydrogen deficient, carbon rich, have extensive dust shells, and each lies at the centre of an old PN.

The final evolution from pre-WD to the BAG phase is predicted to take of the order of a few centuries, thus representing a very rapid (and hence seldom seen) phase of stellar evolution. However, the rate at which Sakurai has evolved has radically changed our views about the post-MS evolution of low- to intermediate-mass (1–8 $M_\odot$) stars, prompting a major rethinking of the underlying astrophysics (Herwig 2001, 2005; Lawlor & MacDonald 2003).

Here we present a series of infrared (IR) observations of Sakurai, obtained with ground-based, airborne, and space-based observatories over the 20-yr period since it became dust embedded in late 1998. We include already-published and unpublished data, and data acquired recently from the NASA *Stratospheric Observatory for Infrared Astronomy* (*SOFIA*; Young et al. 2012; Temi et al. 2014). An overview of the early (1996–2001) IR evolution – including the molecular and dust components – was given by Geballe et al. (2002).

2 SAKURAI'S OBJECT (V4334 SGR): A BRIEF HISTORY OF ITS EVOLUTION

V4334 Sgr was discovered by the amateur astronomer Yukio Sakurai in 1996 (see Nakano, Sakurai & Kojima 1996). Originally reported as a nova, it was at first spectroscopically similar to an F supergiant, possibly with a hot dust shell (Dürbeck & Benetti 1996).

It is now known to be a low-mass ($\sim$0.6 $M_\odot$) post-AGB star that is retracing its post-AGB evolution along the HR diagram following a VLTP (Herwig 2001). This interpretation was strengthened by the discovery that Sakurai lies at the centre of a faint PN 40 arcsec in diameter (e.g. Kerber et al. 1997; Eyres et al. 1998a; Pollacco 1999). Pollacco measured the expansion velocity of the PN shell to be 32 $\pm$ 6 km s^{-1}, which, for a distance of 3.8 kpc (see below), gives a ballistic expansion age of $\sim$11 300 yr. This PN age probably rules out a progenitor having a mass $\lesssim$1.25 $M_\odot$, as the progenitor would not have reached the WD cooling track in the age of the Galaxy. Furthermore, the location of the central star of the PN on the HR diagram in 1995 is incompatible with its being a pre-WD (see Herwig 2001).

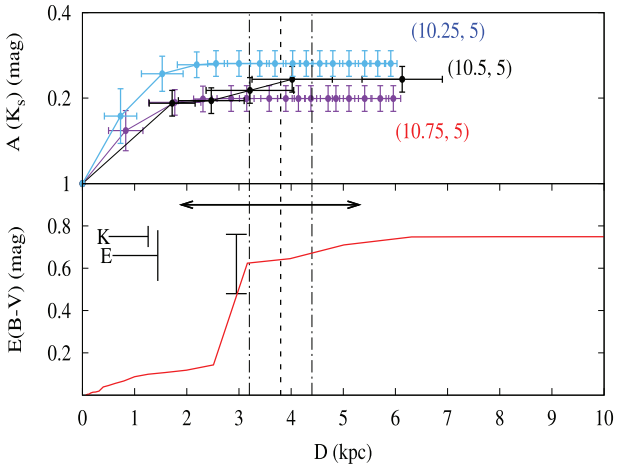

Figure 1. Dependence of reddening $E(B-V)$ (from Green et al. 2018, red curve, bottom panel), and of K_s-band extinction (from Marshall et al. 2006, top panel), on distance. The K_s-band extinction is for three lines of sight close to Sakurai ($l = 10.48°$, $b = +04.41°$); the numbers in brackets give (l, b). The horizontal double-headed arrow gives range of possible distance from Eyres et al. (1998a). The lines labelled 'K' and 'E' give reddening from Kimeswenger (2002) (the weighted mean of several values), and Evans et al. (2002b) (based on strength of the interstellar silicate absorption feature). Error bar at a distance of $\simeq$2.6 kpc gives reddening as determined here. The broken vertical lines depict the adopted distance (3.8 kpc) and associated uncertainties. See Section 4 for details.

In mid-1996, the spectrum of Sakurai rapidly evolved to that of a C-rich, H-poor star, with elemental abundances akin to those found in the R Coronae Borealis (RCB) stars (Asplund et al. 1999). Subsequently, around 1997 April, Sakurai started to produce a carbon dust shell that obscured the central star (see fig. 1 of Dürbeck 2002, for a visual light curve to mid-1999). As the visual light faded, photospheric CO was detectable in the IR until late 1998 but thereafter, even the IR spectrum was completely devoid of photospheric features.

By 1999 April, the photosphere had completely disappeared from view, even at IR wavelengths, and as of early 2020, remains obscured. A large mass-loss rate ($\sim$10^{-5} $M_\odot$ yr^{-1} over the period 1999 May–2001 September) is implied by 1–5 μm spectroscopy (Tyne et al. 2002). Evans et al. (2002a, 2004) detected the dust around Sakurai at 450 and 850 μm in 2001 August, and found that the flux density at these wavelengths was still rising in 2003, indicating that the mass-loss was being maintained; the spectral energy distribution (SED) resembled a blackbody at 360 K.

High-spatial resolution observations using MIDI/VLTI (Chesneau et al. 2009) resolved Sakurai's dust disc, which has an asymmetry that is aligned with the PN reported by Pollacco (1999); the inclination of the dust disc relative to the plane of the sky is $\sim$75°. The mass of dust in the disc was determined to be $\sim$6 $\times$ 10^{-5} $M_\odot$, although this value is somewhat model dependent.

The optical spectrum has shown significant changes since $\sim$2008 (e.g. van Hoof et al. 2015; Van de Steene et al. 2016), when the strength of many emission lines started to increase, most notably [O II] λ7320/7330Å. In addition Van de Steene et al. identify the emergence of electronic transitions of CN at this time, with a likely origin in the dust disc.

On the basis of stellar evolutionary models, Lawlor & MacDonald (2003) suggested that the rapid evolution (on a time-scale of $\sim$10 yr) of Sakurai and V605 Aql – compared with the longer time-scale associated with the evolution of FG Sge – might indicate that the

latter is making its second visit to the AGB, whereas Sakurai and V605 Aql are visiting for the first time. They predicted that the stellar component of Sakurai would rapidly increase in effective temperature, and will eventually resemble V605 Aql, whereas the latter will return to the AGB over the next several decades. That Sakurai and V605 Aql are evolving along similar evolutionary tracks, with V605 Aql somewhat more advanced by virtue of its having undergone a thermal pulse in 1919, was also concluded by Clayton et al. (2006, 2013). Indeed, Clayton et al. suggested that the behaviour of V605 Aql could serve as a template for the future behaviour of Sakurai.

Blöcker (2001) argued that the stellar evolution pathway taken by Sakurai is a fate that awaits 20 per cent of low-mass stars; thus, we are looking at a possible fate of the Sun. Herwig et al. (2011) and others have studied details of the VLTP, and find that the mixing of protons into the He-burning shell can trigger i-process nucleosynthesis, producing the anomalous abundances of species such as Sr, Y, and Zr seen in Sakurai (Asplund et al. 1997). Furthermore, understanding objects that have undergone VLTPs has a much wider significance: There is evidence that carbon stars produce dust in low-metallicity environments, with implications for dust production in (for example) globular clusters and dwarf galaxies (Sloan et al. 2009; Boyer et al. 2015a, b, 2017; Goldman et al. 2019).

3 DUST AND MOLECULES

3.1 The dust

3.1.1 The start of the dust phase

By late 1998, the central star of Sakurai was completely obscured by an optically thick dust shell. Evans et al. (2006) reviewed the expansion of the dust shell by estimating its 'blackbody angular diameter' (see Appendix A). They found that the expansion was linear in time, with an extrapolated start on 1997 November 10 (MJD[1] 50762); the expansion rate was 0.059 mas d^{-1}. Hinkle et al. (2008) determined a similar expansion rate (0.055 ± 0.008 mas d^{-1}) over a somewhat longer time base, also with a start in 1997 November. In either case, the extrapolation to zero diameter coincided with the start of dust production sometime between 1997 November 7 (MJD 50759) and 1998 February 5 (MJD 50849; Dürbeck 2002). However, as noted in Section 2, the IR spectrum shows that dust had actually begun making a contribution to the IR emission as early as 1997 April (Geballe et al. 2002; Pavlenko et al. 2002).

Since 1998, the 1–5 μm continuum SED has crudely resembled a featureless blackbody, commensurate with that emitted by an optically thick carbon dust shell. We will confine our analysis of the dust shell to the period after 1997 November.

3.1.2 The nature of the dust

Analysis of the post-1998 IR observations shows that the dust is carbon based, primarily in an amorphous form (Eyres et al. 1998b; Tyne et al. 2002; Evans et al. 2006). The 1–5 μm spectra during the period 1999–2001 were consistent with mass-loss rate (*in the form of dust only*) that increased steadily from $\sim 5 \times 10^{-8}$ to $\sim 1.8 \times 10^{-7}\,M_\odot\,yr^{-1}$ (see Tyne et al. 2002, for details), where we have scaled as per the DUSTY code (Ivezić & Elitzur 1995) for the distance D and the density of the grain material (see Section 6.3 for the value assumed here). A crude integration of the mass-loss rate (in dust only) over the period 1999–2001 from Tyne et al. (2002) yields the accumulated mass of dust $M_{\rm dust}$ ejected to the end of 2001 to be $\simeq 1.0 \times 10^{-5}\,M_\odot$.

The dust mass over the period 2001 August to 2003 June was determined by Evans et al. (2004) using 850 μm photometry. These authors found that the dust mass increased from 2×10^{-6} to $1.4 \times 10^{-5}\,M_\odot$ over this period (again these values are scaled to the distance assumed here).

The maximum grain radius [in a grain-size (a) distribution $n(a)\,da \propto a^{-q}\,da$, with $q \simeq 3$] increased by a factor of ~ 3 over the period from 1999 May to 2001 September (Tyne et al. 2002).

3.2 The molecules

IR observations (Eyres et al. 1998b) revealed the presence of C_2, CN, and CO through their electronic (C_2; Ballik & Ramsay 1963) and vibrational transitions, including overtone absorption spectra of ^{12}CO and ^{13}CO. The presence of the Ballik-Ramsay bands mirrored the appearance of the C_2 Swan bands (Swan 1857) in the optical (Asplund et al. 1997). The C_2 bands suggested a $^{12}C/^{13}C$ ratio in the range 1.5–5. High-resolution ($R \simeq 30\,000$) spectroscopy (Pavlenko et al. 2004) resolved the first overtone ^{12}CO and ^{13}CO bands, to which Pavlenko et al. fitted a synthetic hydrogen-deficient model atmosphere to determine a $^{12}C/^{13}C$ ratio of 4 ± 1. Both values are substantially less than the Solar system value ($^{12}C/^{13}C = 89$; Lodders et al. 2009). Worters et al. (2009) used the IR CO fundamental bands – seen in absorption against the dust emission – to derive a ratio similar to that of Pavlenko et al. (2004). Evans et al. (2006), using mid-IR HCN lines, also found that the $^{12}C/^{13}C$ ratio is ~ 4.

Tafoya et al. (2017) detected the $J = 4 \rightarrow 3$ transitions of $H^{12}CN$ and $H^{13}CN$, and the $J = 1 \rightarrow 0$ transition of $H^{12}CN$, and found that the expansion velocities were in excess of 100 km s^{-1}. They too found that the $^{12}C/^{13}C$ ratio is extremely low. The consistently low $^{12}C/^{13}C$ ratio in Sakurai – determined from optical, IR, and sub-mm observations – is in line with that expected (~ 3.5; Asplund et al. 1999) from second-stage equilibrium CNO burning following He-burning during the VLTP, and therefore with Sakurai being an object that has undergone a VLTP.

4 REDDENING AND DISTANCE

While the assumed interstellar reddening to Sakurai will have minimal bearing on most of the data we discuss here, there will be a discernible effect at the shortest ($\sim JHK$) wavelengths.

4.1 Distance

A search of the *Gaia* DR2 archive (Gaia Collaboration 2018) reveals no parallax values for Sakurai. Various distance determinations from the literature are summarized by Hinkle & Joyce (2014), in which nearly all estimates lie within the range proposed by Eyres et al. (1998a), namely 1.9–5.3 kpc. As pointed out by van Hoof et al. (2007), the line of sight to Sakurai reaches the scale height of the old disc at $D = 4$ kpc, making this an upper limit (albeit a weak one) on the distance.

We adopt here the 'statistical' distance deduced by Eyres et al. (1998a), namely 3.8 ± 0.6 kpc. We note that the expansion of

[1]Throughout, we use Modified Julian Date (MJD) to identify the time of the observations. MJD is related to Julian Date (JD) by MJD = JD − 2400000.5.

Table 1. Evolution of Sakurai's dust as seen from UKIRT, 2MASS, *WISE*, *Spitzer Space Telescope*, and *SOFIA*. The column headed 'Ref' lists papers containing IR data on Sakurai already published. Observations in the K_s band are listed separately (Table 2). See the text for details.

Facility	Date YYYY-MM-DD	Ref[(a)]	MJD	Wavelength coverage (μm)	$R^{(b)}$	$T_{\rm dust}$ (K)	$[\lambda f_\lambda]_{\rm max}$ (10^{-12} W m^{-2})	$L^{(c)}_{\rm dust}$ (L$_\odot$)	$M^{(c)}_{\rm dust}$ (M$_\odot$)
UKIRT	1998-08-18	1	51043	1.2–2.3		1210 ± 3	1.29 ± 0.01	791 ± 177	5.10[±1.14] × 10^{-10}
″	1999-04-21	2	51289	1.0–2.5	690–950	840.6 ± 0.6	8.16 ± 0.05	5004 ± 1118	1.82[±0.41] × 10^{-8}
2MASS	1999-04-29		51297	$JHK_s^{(d)}$	∼6	950 ± 37	6.57 ± 2.48	4029 ± 1767	8.21[±3.91] × 10^{-9}
UKIRT	1999-05-03	3	51301	1–5	1300–4800	723.5 ± 0.5	14.17 ± 0.12	8689 ± 1942	6.46[±1.44] × 10^{-8}
″	1999-06-08	3	51337	1–5	200–2000	717.1 ± 1.8	14.81 ± 0.23	9081 ± 2033	7.04[±1.58] × 10^{-8}
″	1999-06-14	3	51343	1–5	200–2000	717.2 ± 1.1	14.89 ± 0.04	9130 ± 2039	7.08[±1.58] × 10^{-8}
″	1999-09-06	3	51427	1–5	200–2000	660.9 ± 0.7	15.66 ± 0.11	9602 ± 2145	1.10[±0.25] × 10^{-7}
″	2002-04-14	3	52378	1.4–5	200–2000	432.4 ± 0.3	26.57 ± 0.13	16 292 ± 3639	1.40[±0.31] × 10^{-6}
″	2003-09-08	3	52890	1–5	200–2000	359.6 ± 0.2	12.40 ± 0.05	7604 ± 1698	1.57[±0.35] × 10^{-6}
Spitzer	2005-04-15	4	53475.3	5.2–36	60–600	283.5 ± 0.2	13.17 ± 0.05	8076 ± 1804	5.16[±1.15] × 10^{-6}
″	2007-05-04		54224.9	5.2–33	″	225.5 ± 0.1	9.58 ± 0.03	5874 ± 1312	1.11[±0.25] × 10^{-5}
″	2007-10-15		54388	5.2–33	″	217.0 ± 0.3	9.05 ± 0.05	5549 ± 1240	1.26[±0.28] × 10^{-5}
″	2008-04-08		54564	5.2–33.2	″	205.8 ± 0.2	8.49 ± 0.03	5206 ± 1163	1.53[±0.34] × 10^{-5}
″	2008-10-18		54757.1	5.2–35	″	207.3 ± 0.2	8.52 ± 0.03	5224 ± 1167	1.48[±0.33] × 10^{-5}
WISE	2010-03-19		55274.4	W1, W2, W3, W4[(e), (f)]	1–3	–	–	–	–
SOFIA	2014-03-25		56741.5	8.6–36.6	110–160	181.7 ± 0.6	5.47 ± 0.07	3354 ± 750	1.78[±0.40] × 10^{-5}
″	2016-07-11		57580.3	5.0–31	110–180	176.9 ± 0.5	4.95 ± 0.06	3035 ± 679	1.83[±0.41] × 10^{-5}

Notes. [(a)] 1: Geballe et al. (2002); 2: Tyne et al. (2000); 3: Tyne et al. (2002); 4: Evans et al. (2006).
[(b)] Spectral resolution $R = \lambda/\Delta\lambda$.
[(c)] For $D = 3.8$ kpc.
[(d)] 2MASS pass bands.
[(e)] *WISE* pass bands.
[(f)] Data saturated in W3 and W4; see the text.

the blackbody angular diameter of the dust (see Section 3.1.1), combined with this distance, leads to an expansion velocity for the dust-forming material of ∼375 km s^{-1}; this is comparable with that suggested by the blue wing of the He I 1.0833 μm line in 1997 July (Geballe et al. 2002).

4.2 Reddening

Methods of determining the interstellar reddening, $E(B - V)$, to Sakurai have relied mainly on measuring the Balmer decrement. An early determination using this method was made by Dürbeck & Benetti (1996), who found $E(B - V) = 0.54$ mag. However, more recent considerations have deduced larger reddening. Kimeswenger (2002) gives a weighted mean, based on several independent determinations up to 2002, of 0.75 ± 0.05 mag. Evans et al. (2002b) reported a detection of the 9.7 μm silicate feature in absorption in Sakurai. They argued that the feature actually arises in the interstellar medium, and therefore provides a direct measure of the reddening by interstellar material, $E(B - V) = 0.66 \pm 0.12$ mag. van Hoof et al. (2007) found $E(B - V) = 0.86$ mag from the Balmer decrement, assuming that 'Case B' applies.

Marshall et al. (2006) have used the Two Micron All Sky Survey (2MASS; Skrutskie et al. 2006) catalogue to map out the Galactic extinction in the K_s (2.159 μm) band; in the direction of Sakurai, their data indicate $A_{K_s} \simeq 0.20$–0.24 mag for the range of distances suggested by Eyres et al. (1998a), as depicted in Fig. 1. A weighted mean of the A_{K_s} values in Marshall et al., over the Eyres et al. distance range, gives $A_{K_s} \simeq 0.22 \pm 0.03$ mag. This value of extinction is consistent with the extinction analysis by Gonzalez et al. (2012), who found $E(J - K) = 0.312 \pm 0.115$ mag and $A_K = 0.216$ mag towards Sakurai. The A_{K_s} value of 0.22 ± 0.03 mag corresponds to $E(B - V) = 0.61 \pm 0.07$ mag, close to the value derived by Evans et al. (2002b).

These considerations suggest that determinations of the reddening using the Balmer decrement and Case B may overestimate $E(B - V)$. On the other hand, determining the reddening using only the agents of interstellar extinction points to a consistent $E(B - V) = 0.61 \pm 0.07$ mag (A_{K_s} extinction) and $E(B - V) = 0.66 \pm 0.12$ mag (9.7 μm feature). For the purposes of this paper, we use a weighted mean of the reddening as deduced from the interstellar extinction only, namely $E(B - V) = 0.62 \pm 0.06$ mag.

5 THE DATA

We have compiled a series of IR observations – both photometric and spectroscopic – that show the dust emission by Sakurai, covering the period from 1996 April to 2016 July, providing a 20-yr retrospective of IR observations of the dust evolution of a VLTP. We briefly describe the observations here. An observing log is given in Table 1 and a sample of the spectroscopic data, together with blackbody fits (discussed in Section 6 below), is shown in Fig. 2.

5.1 UKIRT

Sakurai was observed with the United Kingdom Infrared Telescope (UKIRT) from 1996 to 2000. Full details of the spectrometers used, data acquisition and reduction, together with the data themselves, are given in Eyres et al. (1998b), Pavlenko et al. (2004), and Tyne et al. (2002) and references therein.

5.2 K_s-band photometry

Archival data on Sakurai have been retrieved from the European Southern Observatory's *VISTA Variables in the Vía Láctea* survey (Saito et al. 2012) and are listed in Table 2, which also includes data from Hinkle & Joyce (2015; see that paper for instrumental details) and Hinkle, Joyce & Matheson (2017). The observations on MJD 55457.25/55458.21 were combined into a single image, which shows both a bright point source and ejecta. Aperture photometry

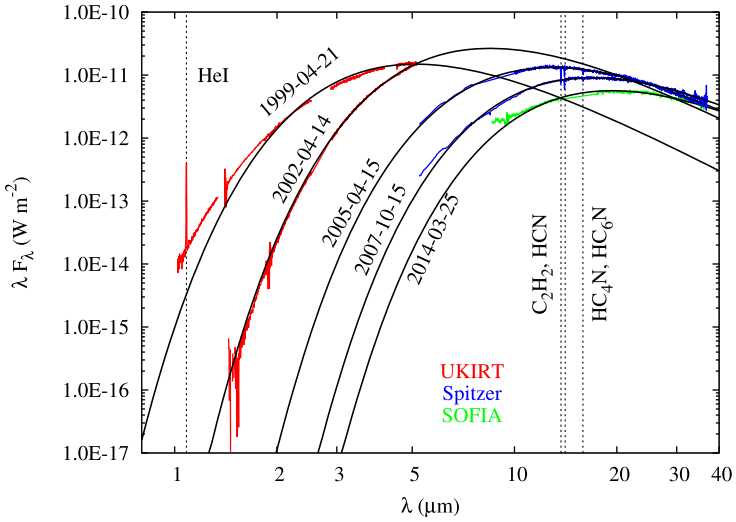

Figure 2. Selected snapshots of the evolution of the SED of Sakurai's dust shell, obtained on the dates indicated and with the facilities shown, from 1999 to 2014. Note the poor atmospheric transmission in the UKIRT data at wavelengths ∼1.4 and ∼1.8 μm. A warm dust contribution, not shown, is present in the near-IR in 2014-03-25 (see Section 6.5). Curves are labelled with the dates of observation; see Table 1 for further details. Wavelengths of the He I 1.083 μm line, and the hydrocarbon lines, are indicated.

Table 2. K_s-band observations of Sakurai. See the references below for full details.

MJD	K_s (mag)	Ref	Comment
54984.79	>18.4	2	3σ limit
55298.27	17.45 ± 0.28	1	–
55457.25	–	–	Average of
55458.21	16.38 ± 0.15	2	two nights
55726.31	15.89 ± 0.09	1	–
55777.19	15.63 ± 0.06	1	–
55791.09	15.68 ± 0.06	1	–
55807.08	15.70 ± 0.07	1	–
55823.06	15.52 ± 0.05	1	–
55831.01	15.56 ± 0.06	1	–
56408.53	13.98 ± 0.04	2	–
56555.10	14.03 ± 0.02	2	–
56729.52	13.98 ± 0.04	2	–
56816.33	13.80 ± 0.01	2	–
57584.91	13.35 ± 0.02	3	–
57975.07	13.20 ± 0.02	1	–

Notes. 1. Data from VISTA InfraRed CAMera on the 4-m Visible and Infrared Survey Telescope for Astronomy (VISTA). See Saito et al. (2012).
2. Data obtained with the High-Resolution Infrared Camera on the Kitt Peak National Observatory (KPNO) 3.5-m telescope, the Extremely Wide-Field Infrared Imager on the KPNO 4-m telescope, and with the Near InfraRed Imager and spectrograph (NIRI) on the Gemini North telescope. See Hinkle & Joyce (2015).
3. Data obtained with NIRI. See Hinkle et al. (2017).

was obtained on both images and the fluxes were combined to get the measured magnitude. The data are plotted in Fig. 3.

5.3 2MASS

Sakurai is included in the 2MASS survey, with fluxes of 38.08 ± 0.66, 341.27 ± 9.24, and 1884 ± 19 mJy in the J (1.235 μm), H (1.662 μm), and K_s (2.159 μm) bands, respectively.

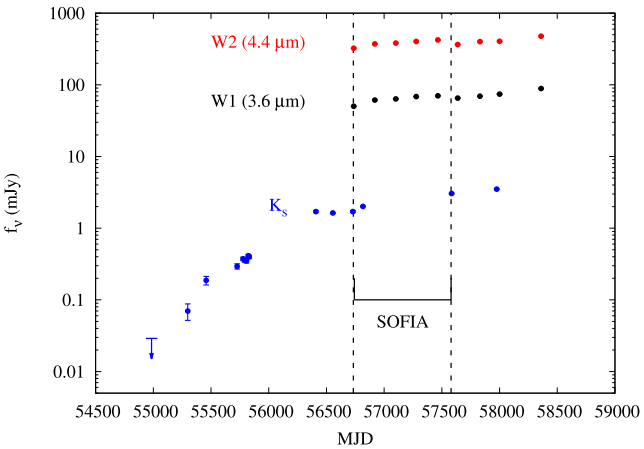

Figure 3. K_s band (blue), *NeoWISE* bands *W1* (black) and *W2* (red) light curves of Sakurai. Times of the *SOFIA* observations discussed in Section 5.6 are indicated; see Section 6.5 for discussion of data highlighted by the dotted vertical line.

The data are for the epoch 1999 April 29 (MJD 51297) and are shown in Fig. 4.

5.4 *WISE*

Sakurai was observed in 11 scans during the Wide-field Infrared Survey Explorer (*WISE*; Wright et al. 2010) survey during an ∼1 d interval centred around MJD 55274.4. The mean survey magnitudes were 10.77 ± 0.09, 7.79 ± 0.02, 0.17 ± 0.15, and −2.03 ± 0.01 mag in the *WISE* bands *W1* (3.3 μm), *W2* (4.6 μm), *W3* (12 μm), and *W4* (22 μm), respectively; the corresponding flux values were 15.13 ± 1.19 mJy (*W1*), 131.14 ± 2.54 mJy (*W2*), 24.84 ± 3.52 Jy (*W3*), and 53.63 ± 0.05 Jy (*W4*).

However, the *WISE* survey data suffer from saturation at magnitudes brighter than 8.1 (*W1*), 6.7 (*W2*), 3.8 (*W3*), and −0.4 (*W4*); the survey magnitudes for Sakurai indicate that the *WISE* photometry in

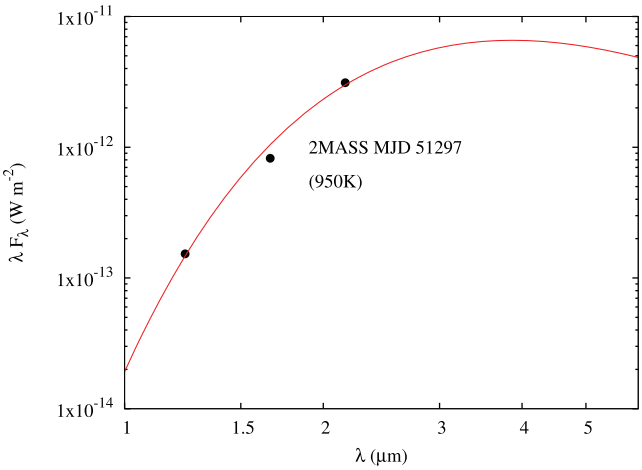

Figure 4. SED of Sakurai from the 2MASS survey photometry; the red curve is blackbody fit.

bands *W3* and *W4* is affected by saturation, with 30 and 20 per cent of pixels, respectively, affected. Although data in the *W1* and *W2* bands are less affected by saturation, we do not use data from the *WISE* cryogenic survey here; they are included in Table 1 for completeness.

Although the *WISE* survey was completed in 2010 September with the exhaustion of the cryogen, the mission was extended using bands *W1* and *W2* only to produce the *NeoWISE* survey (Mainzer et al. 2014). Sakurai was ∼1 mag brighter in both the bands *W1* and *W2* during the *NeoWISE* survey (9.18 ± 0.02 and 6.8 ± 0.01 mag, respectively) than it was ∼6 yr earlier, during the main *WISE* survey (*W1* and *W2* magnitudes 10.77 ± 0.09 and 7.79 ± 0.02 mag, respectively). The *NeoWISE* data do not suffer from saturation, and we note from Cutri et al. (2012) that no correction to the photometry is needed in these data. The averaged daily *NeoWISE* scans are shown in Fig. 3.

5.5 *Spitzer Space Telescope*

Sakurai was observed on several occasions (Program IDs 3362, 30077, and 40061; PI: A. Evans) in the period 2005–2008 with the Infrared Spectrometer (IRS; Houck et al. 2004) on the *Spitzer Space Telescope* (Werner et al. 2004; Gehrz et al. 2007). Spectra were obtained in both low- and high-resolution modes, covering the spectral range of 5–38 μm. In order to treat the data in a coherent and systematic way, we have used the data provided by the Combined Atlas of Sources with the *Spitzer* IRS spectra (CASSIS; Lebouteiller et al. 2011, 2015).

5.6 *SOFIA*

Spectra of Sakurai were obtained with *SOFIA* using the Faint Object infraRed CAmera for the *SOFIA* telescope (FORCAST; Herter et al. 2012, 2013). The observations were carried out on two flights, on 2014 March 25 (flight F155, Palmdale, California, Cycle 2 programme 02_0024; PI: A.Evans) and on 2016 July 11 (flight F318, Christchurch, New Zealand, Cycle 4 programme 04_0003; PI: A. Evans). Sakurai was observed with the grisms, slits, and on-target integration times listed in Table 3. Observations were generally carried out with the 4.7-arcsec slit; one observation on flight F318 used the 2.4-arcsec slit with the G063 grism. All observations used the default two-position chopping with nodding mode.

The FORCAST scientific data products were retrieved from the *SOFIA* archive, after standard pipeline processing and flux calibration were performed (for details, see Clarke, Vacca & Shuping R. 2014). An extensive discussion of the FORCAST data pipeline can be found in the Guest Investigator Handbook for FORCAST Data Products, Rev. B.[2]

We note here that the slit widths in both the *Spitzer Space Telescope* and *SOFIA* spectroscopic observations are such that any contribution from the 40-arcsec PN (see Section 2) is negligible.

6 DUST EMISSION

6.1 The SED

It is almost certain that the dust shell around Sakurai contains dust grains that have a range of temperatures. Even so, the observed SED of the dust resembles emission by a blackbody, particularly after 1998. We have therefore fitted

$$f_\lambda = \frac{F}{\lambda^5}\,\frac{1}{\exp[B/\lambda]-1} \tag{1}$$

to the photometric and spectral data, where $T_{\rm dust}$ is the observed dust temperature, and B ($= hc/kT_{\rm dust}$) and F are the constants to be determined. Obvious 'glitches' in the data, possible and actual spectral features (such as HCN; Evans et al. 2006, and see below), as well as spectral regions where the quality of the data is clearly poor, were removed before fitting.

A sample of the fits for the de-reddened UKIRT, *Spitzer Space Telescope*, and *SOFIA* data is shown in Fig. 2. Clearly, in some cases the fit is poor at wavelengths $\lesssim$2 μm, reflecting the fact that the emission in these cases is not well described by a simple blackbody. Indeed, there is clear evidence in the earliest spectra of the presence of a photospheric contribution that diminishes with time.

The observed emitted power f and dust luminosity $L_{\rm dust}$ were determined from (see Appendix A)

$$[\lambda f_\lambda]_{\rm max} = F\left(\frac{\alpha}{B}\right)^4 \frac{1}{e^\alpha - 1}$$
$$f = 1.359\,[\lambda f_\lambda]_{\rm max}$$
$$L_{\rm dust} = 4\pi D^2 f,$$

where $\alpha \simeq 3.92$. We use the fitted parameters B and $T_{\rm dust}$ to determine $[\lambda f_\lambda]_{\rm max}$ as in most cases the wavelength at which $[\lambda f_\lambda]$ is a maximum falls outside the data wavelength range, or in a gap in the data. In doing so, we risk missing some emission; however, the SED of Sakurai, using the near-contemporaneous UKIRT and JCMT data from late 2003 (Evans et al. 2004), suggests that the 1–5 and 450/850 μm emission lies on the same blackbody curve. Thus, we are confident that we are not excluding any emission, for example by cold dust. The deduced values of $T_{\rm dust}$, $[\lambda f_\lambda]_{\rm max}$, and $L_{\rm dust}$ are given in Table 1.

We note that the uncertainties in $T_{\rm dust}$ in Table 1 are the formal uncertainties resulting from fitting equation (1) to the data, and are not therefore 'physically' meaningful. As already noted the dust shell will include a range of temperatures that far exceed the limits implied by the errors listed. However, we use these errors to estimate the uncertainties in the dust mass. Likewise, the uncertainties in $L_{\rm dust}$ include the uncertainties in both $[\lambda f_\lambda]_{\rm max}$ and

[2]https://www.sofia.usra.edu/Science/DataProducts/FORCAST_GI_Handbook_RevA1.pdf

Table 3. Log of *SOFIA* FORCAST observations.

Flight	Date YYYY-MM-DD	Filter	Slit (arcsec)	Wavelength coverage (μm)	Nominal resolution R	Exposure time (s)
F155	2014-03-25	G111	4.7	8.4–13.7	130	1500
		G227	4.7	17.6–27.7	110	100
		G329	4.7	28.7–37.1	160	100
F318	2016-07-11	G063	2.4	4.9–8.0	180	1500
		G111	4.7	8.4–13.7	130	1500
		G227	4.7	17.6–27.7	110	50
		G329	4.7	28.7–37.1	160	500

D. It is interesting to note that Evans et al. (2004) fitted a 360 K blackbody to the UKIRT/JCMT data by eye; the formal fit to the UKIRT data (Table 1) gives 359.6 ± 0.2 K.

Although there are only three photometric points in the 2MASS data, they all lie on the Wien tail of a blackbody and a fit to the data gives $T_{\rm dust} = 950 \pm 37$ K, and $[\lambda f_\lambda]_{\rm max} = 6.6[\pm 2.5] \times 10^{-12}$ W m^{-2}. The 2MASS SED is shown in Fig. 4, and the dependence of $T_{\rm dust}$, $[\lambda f_\lambda]_{\rm max}$, and $L_{\rm dust}$ on time is shown in Fig. 5.

6.2 The dust temperature

There is a monotonic decline in $T_{\rm dust}$, from ∼1200 to ∼180 K over the period from 1998 August to 2016 July. We note that the observed dust temperature has been well below the formation temperature for amorphous carbon (∼1000 K; see Gehrz et al. 2018, and references therein) since 1999.

For the simple case of dust moving away at a constant speed from a source of bolometric luminosity $L_*(t)$, we would expect the dust temperature to vary as $T_{\rm dust} \propto (L_*(t)/t^2)^{1/(\beta+4)}$, where β is the 'β-index' for the dust material (see below; see Bode & Evans 1989; Evans 1993, for derivations). We therefore explore the possibility that the dust temperature declines with power-law dependence on time according to

$$T_{\rm dust} = \frac{C}{({\rm MJD} - {\rm MJD}_0)^\gamma}, \tag{2}$$

where C, MJD$_0$ (the epoch at which the mass-loss leading to dust condensation started), and γ are the constants to be determined; note that this expression implicitly assumes a constant L_*.

We have already noted that the drop in the optical brightness began as early as late 1997. Fitting equation (2) to the data gives

$$C = 3.38[\pm 6.95] \times 10^6$$
$$\gamma = 1.14 \pm 0.23$$
$$\mathrm{MJD}_0 = 49736 \pm 491$$

for $T_{\rm dust}$ in K (from Table 1) and MJD, MJD$_0$ in days. The parameters MJD$_0$ and γ are reasonably well constrained, while C is not; this may be a reflection of the fact that L_* is indeed time dependent. We revisit MJD$_0$ below.

6.3 The dust mass

Tyne et al. (2002) fitted DUSTY (Ivezić & Elitzur 1995) models to the UKIRT data covering the period 1999 May 4–2001 September 8. Assuming a gas-to-dust ratio of 200, they deduced a mass-loss rate that increased from $\sim 5 \times 10^{-6}$ M$_\odot$ yr^{-1} at the earlier time to $\sim 12 \times 10^{-6}$ M$_\odot$ yr^{-1} at the later time. However, the gas-to-dust ratio in Sakurai's environment is almost certainly very different from that assumed by Tyne et al.

If we make the working assumption that the dust disc enveloping Sakurai is optically thin at longer ($\gtrsim$5 μm) wavelengths and at later times, then we can employ the method used by Gehrz et al. (2015) and Evans et al. (2017) to estimate the dust mass, which is given by (see those papers for details)

$$\frac{M_{\rm dust}}{{\rm M}_\odot} = 4.81 \times 10^{16} \left[\frac{[\lambda\, f_\lambda]_{\rm max}}{{\rm W\ m^{-2}}}\right] \left[\frac{D}{\rm kpc}\right]^2 \times \left[\frac{\rho}{\rm kg\ m^{-3}}\right] \frac{1}{A\, T^{(\beta+4)}}. \tag{3}$$

Here, ρ is the density of the grain material (1500 kg m^{-3} for amorphous carbon, which we assume here; Jones et al. 2017), and the constants A and β are defined such that the Planck mean absorption efficiency is given by $\langle Q_{\rm abs}\rangle = AaT^\beta$, with a being the grain radius. For amorphous carbon, $A = 58.16$ when a is in cm, and $\beta = 0.754$ (Evans et al. 2017). Obviously, the calculated dust masses can be scaled appropriately if a different density is used for amorphous carbon. For a distance of 3.8 kpc, the dust mass is

$$\frac{M_{\rm dust}}{{\rm M}_\odot} = 1.79 \times 10^5 \left[\frac{[\lambda\, f_\lambda]_{\rm max}}{10^{-12}\ {\rm W\ m^{-2}}}\right] T^{-(\beta+4)}.$$

We use the data in Table 1 to find the dust masses in the final column. The uncertainties in $[\lambda\, f_\lambda]_{\rm max}$, T, and D are propagated into the uncertainties in $M_{\rm dust}$; however, there are likely to be substantial uncertainties in both A and ρ, which will make a (possibly) large (and unquantifiable) contribution to the uncertainties in Table 1.

The dependence of $M_{\rm dust}$ with time is shown in Fig. 5. We see a clear and sustained increase in the dust mass from the time of formation in late 1997, until it levels off after MJD ∼55000 (mid-June 2009). In Fig. 5, we include the dust mass determined by Evans et al. (2004) (see Section 3.1.2); although determined using rather different methods, the dust masses deduced here and in Evans et al. are reasonably consistent.

Unlike the case for the dust temperature, there is no physically based expression for the time dependence of dust mass. For our present purpose, we fit a function of the form[3]

$$\frac{M_{\rm dust}}{10^{-10}\ {\rm M}_\odot} = \exp\left\{K\ \ln 10 \times \left(1 - \exp\left[-\frac{({\rm MJD} - {\rm MJD}_0)}{\tau_0}\right]\right)\right\} \tag{4}$$

to the variation of $M_{\rm dust}$ with MJD time, where K, τ_0, and MJD$_0$ (as before, the time of onset of mass-loss) are the constants to be

[3]The reason for this choice of function is that it results in a manageable time dependence of the form$\log_{10}[M_{\rm dust}] \propto (1 - \exp[-t/\tau_0])$.

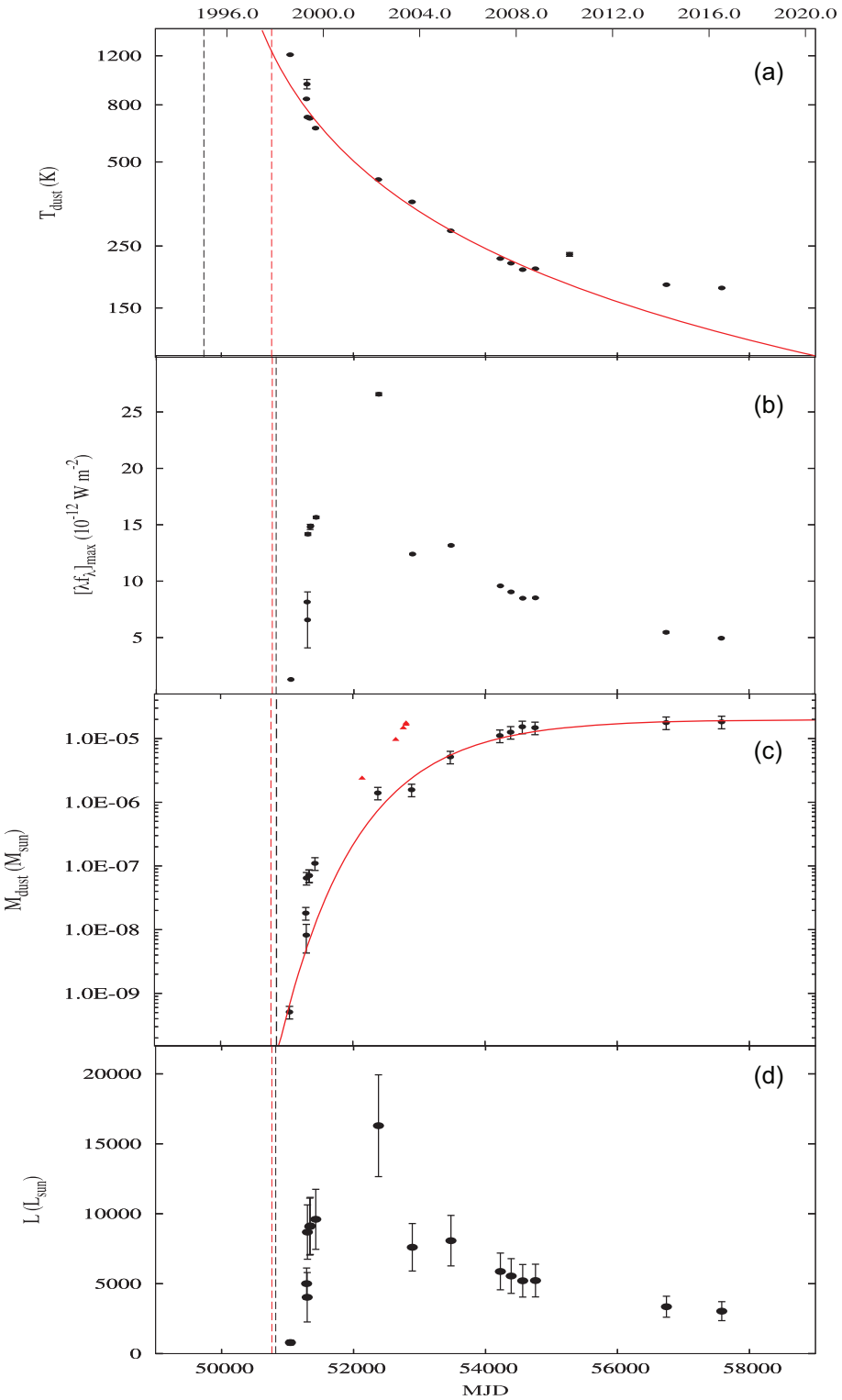

Figure 5. Evolution of Sakurai's dust shell. (a) blackbody temperature of the dust; (b) $[\lambda f_\lambda]_{max}$; (c) dust mass; the red points are from Evans et al. (2004), scaled to $D = 3.8$ kpc; (d) the bolometric luminosity of the dust. The red curves are fits as described in the text. The broken vertical black lines in (a) and (c) are epochs of dust formation as determined separately for dust temperature and dust mass; the broken vertical lines in (b) and (d) are the weighted mean of epoch of dust formation as discussed in the text. The broken vertical red lines are epoch of zero dust shell angular diameter, as determined by Evans et al. (2006).

determined.[4] We find that (with $M_{\rm dust}$ in $\rm M_\odot$ and MJD in days)

$$K = 5.30 \pm 0.16$$
$$\tau_0 = 1167 \pm 179 \text{ d}$$
$$\text{MJD}_0 = 50846 \pm 76$$

give a passable fit to $M_{\rm dust} - t$ (see Fig. 5). These values will depend somewhat on the form of the function assumed, but we might reasonably expect that the value of MJD_0 deduced here is consistent with that deduced from the time dependence of the dust temperature (49736 ± 491; see above); this they do, within the uncertainties. A weighted mean gives

$$\text{MJD}_0 = 50820 \pm 75.$$

The mean value of MJD_0 corresponds to 1998 January 7, but the uncertainty allows the onset of the mass ejection that led to dust formation to have occurred between MJD 50745 (1997 November 24) and MJD 50895 (1998 March 23). This is close to the time at which the expansion of the dust shell started, on $\text{MJD}_0 = 50762$ (Evans et al. 2006; Hinkle et al. 2008).

As noted above, the values of K, τ_0, and MJD_0 must depend on the form of the function assumed for the fitting. Nevertheless, from equation (4) we might expect that the dust mass approaches $10^{(K-10)}\,\rm M_\odot$ as MJD $\rightarrow \infty$, i.e. $M_{\rm dust}(t \rightarrow \infty) \simeq 2.0 \times 10^{-5}\,\rm M_\odot$. We also note that the dust mass on 2007 May 4 (MJD 54224.9, close to the time of the VLTI observation of Chesneau et al. 2009, MJD 54280) was $\sim 1.1 \times 10^{-5}\,\rm M_\odot$, somewhat less than the value given by Chesneau et al.

In principle, the time derivative of $M_{\rm dust}$ in equation (4) might give the mass-loss rate, in the form of dust, and scaling for an appropriate gas-to-dust ratio would give the overall mass-loss rate. However, given that (a) the formula assumed is for mathematical convenience and has no physical basis (see footnote 3), (b) the gas-to-dust ratio will likely change with time, and (c) the deduced mass-loss in the form of dust alone might be due to grain growth rather than grain formation, this approach would not lead to a credible result. Indeed, it is clear that the steep rise in the value of $M_{\rm dust}$ at the start of the dust phase results in a ferocious mass-loss rate, in dust alone. This leads us to suspect that the dust masses deduced – at least at the earlier times – do not accurately reflect the dust mass in Sakurai's environment. This is most likely because the dust emission is not as simple as we have supposed here, and is unlikely to be optically thin at the shortest wavelengths ($\lesssim$5 μm), particularly after mid-1998 when the visual light curve had entered the very deep minimum. Tyne et al. (2002) concluded that the visual optical depth at these times is ∼9, leading to an optical depth of ∼2 at 2.2 μm for any plausible extinction law. It is possible that the dust mass is underestimated at the early times, when the *UKIRT* observations were carried out.

We also note that determining the mass of circumstellar material, or the mass-loss rate, from the dust parameters by assuming a specific gas-to-dust ratio (see e.g. Tyne et al. 2002) will almost certainly lead to erroneous values because the gas-to-dust ratio is (a) unknown and (b) almost certainly variable.

[4]Equation (4) leads to the somewhat spurious result that the dust mass $=10^{-10}\,\rm M_\odot$ at MJD_0. This of course is a consequence of our choice of function, as described in Footnote 3. This has no effect on our conclusions.

6.4 The emitted power

The power emitted by the dust (see Fig. 5) seems to rise sharply after dust condensation began, reaching a maximum around MJD 51350, and then declining (see Fig. 5). There appears to be a sharp peak in $L_{\rm dust}$ at around MJD 52378. However, as noted above (Section 6.3), it is very likely that the dust is optically thick at the shorter IR wavelengths at the earliest times so that the $L_{\rm dust}$ at these times is underestimated. This accentuates the sharpness of the peak in luminosity.

Although the dust shell is optically thick at visible wavelengths – so that the dust shell could act as a 'calorimeter' that monitors the luminosity of the (invisible) central star – we should be cautious of concluding anything about the behaviour of the central star from these data. This is because interferometric observations (Chesneau et al. 2009) show that the dust is distributed in a torus rather than completely enveloping the star, so that an unknown (and almost certainly variable) fraction of the star's radiation 'leaks out' of the dust shell, along the axis of the torus and therefore away from our line of sight. The luminosity values in Table 1 – in which the errors include the uncertainties in $[\lambda f_\lambda]_{\rm max}$ and D – are therefore lower limits on the stellar luminosity, L_*: $L_{\rm dust} = \phi L_*$, where $\phi \leq 1$.

However, if we suppose that the same fraction of the star's light leaks out over the period 2005–2016, then the relative changes in the $L_{\rm dust}$ values in Table 1 might reflect the relative changes in the actual stellar luminosity. The $L_{\rm dust}$ values in the table decline from ∼16 000 to ∼3000 $\rm L_\odot$ over an 11.25-yr period. Hajduk et al. (2005) have presented an evolutionary track for Sakurai. This suggests that the bolometric luminosity is expected to decrease from $\log[L_*/\rm L_\odot] \sim$ 4.2 to 4.1 over a similar period, compared with a decline in $L_{\rm dust}$ from $\log[L_{\rm dust}/\rm L_\odot] = 4.21$ to 3.48: The observed decline is by a factor of ∼5.4, compared to the predicted decline of ∼1.25. However, for the reasons outlined above, our deduced dust luminosities are almost certainly lower limits, so a comparison with stellar evolution models should not be taken too far.

6.5 A fresh ejection event after 2008 October

Apart from a contribution from the stellar photosphere at the earliest times (see Fig. 2), the SED of the dust shell is generally well represented by a simple blackbody from 1999 to 2007. In the latest (*SOFIA* FORCAST) data, however, while the data for $\lambda \gtrsim 10$ μm are well described by a single blackbody, there appears to be an excess at the shorter ($\lesssim$10 μm) wavelengths (see Fig. 6; note that it is the properties of the cooler dust that are tabulated in Table 1 and illustrated in Fig. 5). Furthermore, both sets of *SOFIA* data were obtained within days of the K_s and *NeoWISE* data, and latter data sets confirm the excess seen by *SOFIA* (see Fig. 3).

We also note that, in addition to the $\lesssim$10 μm excess, there might be a small K_s-band excess in the latest SEDs (see Fig. 6), so there might be a small stellar contribution to the K_s flux (see Section 5.2). This suggests that the stellar photosphere might be finally beginning to peer through the gloom. However, the contribution can only be a minor one, and there can be no doubt that the great majority of this late $\lesssim$10 μm excess is primarily due to emission by dust.

Using the same procedure as in Section 6.3, and again assuming amorphous carbon, we determine the mass and temperature of the dust responsible for the near-IR excess. We find that the mass and temperature of the dust in 2014 March were $2.6[\pm 0.4] \times 10^{-8}\,\rm M_\odot$ and 437[±3] K, respectively; in 2016 July, these parameters had the values $5.7[\pm 1.0] \times 10^{-8}\,\rm M_\odot$ and 411[±6] K, respectively.

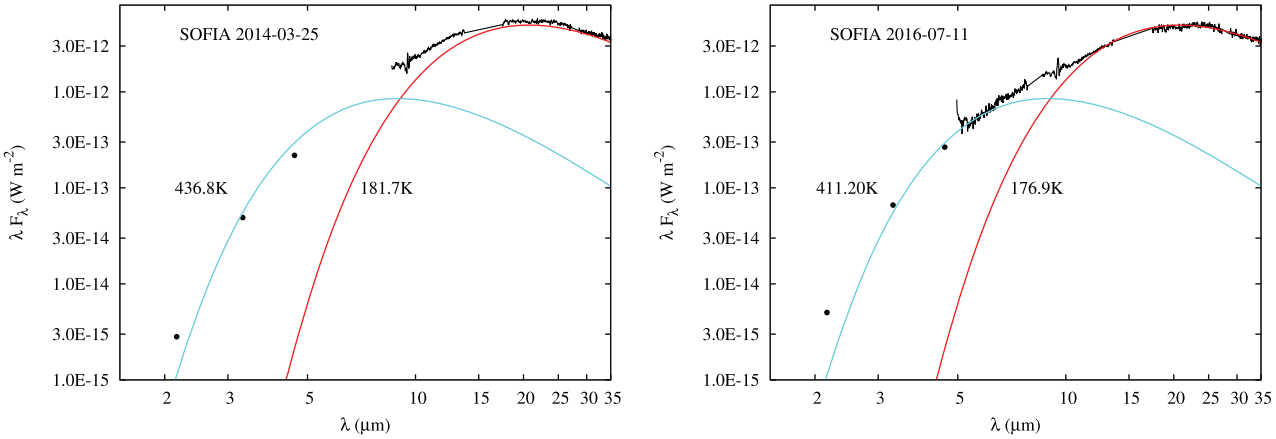

Figure 6. Evidence for the formation of fresh dust. The *SOFIA* FORCAST data for both 2014 March 25 and 2016 July 11 show an excess relative to the fitted blackbody at wavelengths $\lesssim$10 μm. The black points are near-contemporaneous K_s and *NeoWISE* photometry. Temperatures of the blackbodies, which are fitted separately to the long wavelength data and the near-IR excess, are indicated. See the text for details. The apparent 'feature' just short of 10 μm in the *SOFIA* data is the result of incomplete removal of telluric ozone.

The substantial rise in the K_s-band flux from ∼2009 to 2017 (Fig. 3), coupled with the rise in the *NeoWISE* band *W1* and *W2* fluxes between 2010 and 2016 (Section 5.4 and Fig. 3), the apparent increase in dust mass, and the cooling of the 'new' dust between 2010 and 2014–16, all point to renewed, and possibly substantial, mass-loss since ∼2008. The constancy of the molecular column densities from 2005 April to 2008 October (see Section 8 below) suggests that the onset of this most recent mass-loss episode must have occurred after 2008 October.

The mass of the fresh dust is some three orders of magnitude smaller than that of the dust formed in the first mass-loss episode (cf. Table 1). However, if the fresh dust formation episode follows the same pattern as the earlier event, it does not augur well for our prospects of seeing the stellar photosphere any time soon.

7 POSSIBLE DUST FEATURES

We consider here the possibility that there might be dust features, either in emission or in absorption in the mid-IR spectra of Sakurai.

In Fig. 7 (left-hand panel), we show the *Spitzer* IRS spectra for three epochs, together with a 250 K blackbody curve for comparison. The latter is obviously smooth, whereas the *Spitzer* spectra are not. There are weak inflections in the data that hint at the presence of features in either absorption or emission. The putative features are too broad to be atomic/ionic, and do not have the profiles expected of molecular features. Also, in Fig. 7 (right-hand panel) the same data are displayed as $f_\nu/f_{\rm BB}(T)$, where T is the temperature of the best-fitting blackbody from Table 1, to highlight these features (unfortunately, the *SOFIA* data are too noisy in this spectral region to confirm the presence of the features).

While it might be possible to choose a better continuum to bring out the features, it is clear that the overall spectral shape is the same for all three epochs in Fig. 7. We consider that they are weak absorption features, with maximum absorption at ∼6.3 and $\gtrsim$7.5 μm, and a weaker feature longward of ∼7 μm. A plausible identification is with hydrogenated amorphous carbon (HAC), and specifically nitrogenated HAC (see below).

García-Hernández, Kameswara Rao & Lambert (2013) have identified similar (weak) features in the *Spitzer* IRS spectra of RCB stars. They find that these features are somewhat different in the 'hydrogen-rich' RCB stars and in the more common 'hydrogen-deficient' RCB stars. The former have features at ∼6.27, ∼6.6, ∼7.02, and ∼7.7 μm, rather similar to those we identify in Sakurai.

Laser vaporization of graphite in an H_2/N_2 gas mixture gives rise to features in the 6.0–6.5 μm range and a weaker feature at ∼7.0 μm, together with broad absorption going from ∼7.5 μm to longer wavelengths (Grishko & Duley 2002), just as we see in Sakurai. As we discuss in Section 8 below, we see HCN, HNC, and other small hydrocarbon molecules in absorption against the dust shell. Given that there have been at least two dust ejection events in the past ∼20 yr (see Section 6.5), the absorbing material may arise in material from an even earlier ejection event. The possible nitrogenation of the HAC also seems consistent with the presence of N-bearing molecules.

The observational (García-Hernández et al. 2013) and laboratory evidence (Grishko & Duley 2002) seems therefore to point to the existence of a cooler, hydrogen-rich carbon dust shell outside the dust shell that is prominent in the near- and mid-IR.

8 MOLECULAR ABSORPTION

Evans et al. (2006) reported the detection of a number of small hydrocarbon molecules in the *Spitzer* spectrum of Sakurai; these are listed in Table 4 and illustrated in Fig. 8. To the list in Evans et al., we have added a number of new identifications, which are further discussed below.

In Evans et al. (2006), we used a simple model to estimate the column densities and temperatures of the $H^{12}CN$, $H^{13}CN$, and C_2H_2 molecules, and we reprise this exercise here. We determine the continuum in the region of each feature by fitting a linear function $F_\nu(\mathrm{Jy}) = a_0 + a_1\lambda(\mu\mathrm{m})$, whence the wavelength dependence of the optical depth τ is obtained. The typical uncertainty in τ is ±0.02, as determined by the rms value of the 'zero' τ in the 13–15 μm range. The optical depth is fitted assuming that the absorbing gas is homogeneous and isothermal, in thermodynamic equilibrium, and located in a plane-parallel slab in front of the dust. Individual transitions are assumed to have intrinsic widths determined by the velocity widths of the HCN isotopologues measured by Tafoya et al. (2017) ($\simeq$300 km s^{-1}).

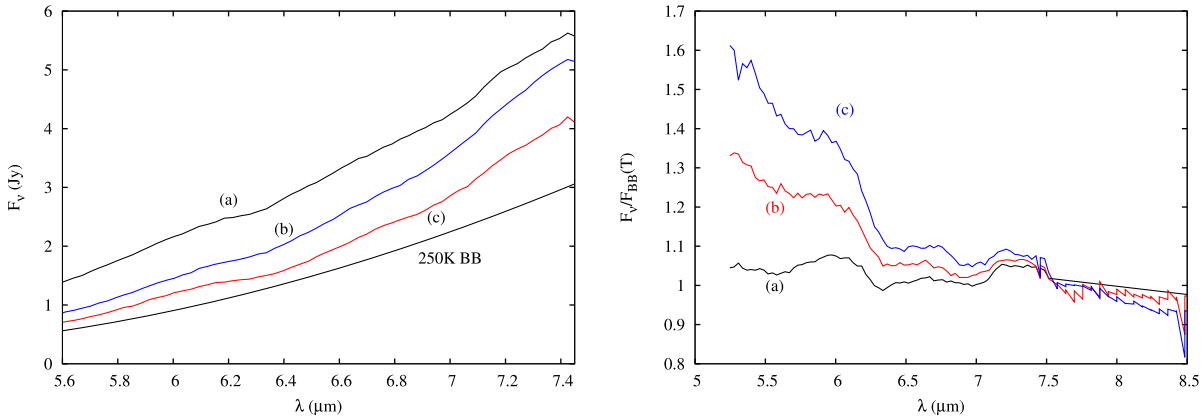

Figure 7. Left: *Spitzer* spectra of Sakurai in the region 5.6–7.4 μm for (a) 2005-04-15 (283.5 K), (b) 2007-05-04 (225.5 K), and (c) 2007-10-15 (217.0 K). A 250 K blackbody, arbitrarily normalized, is shown for comparison. Right: Data from the left-hand panel, rectified by fitted blackbodies as discussed in the text, to bring out the weak features; labelling of curves is as per the left-hand panel.

Table 4. Hydrocarbon and other small molecules in Sakurai as observed by *Spitzer*. $H^{12}CN$ transitions from Aoki, Tsuji & Ohnaka (1999); HNC transitions from Harris et al. (2002). Tentative identifications are indicated by a '[?]'.

Molecule	λ_{obs} (μm)	Band	λ_{id} (μm)
C_2H_2	13.69	ν^5 Q branch	–
$H^{12}CN$	14.03	$2\nu_2^2 - 1\nu_2^1$	14.00
$H^{12}CN$	–	$1\nu_2^1 - 0\nu_2^0$	14.04
$H^{13}CN$	14.14	Q	14.16
HC_4H	15.92	ν_8	15.93
HC_6H	16.09	ν_8	16.07
″	–	ν_{11}	16.10
HNC	21.61	–	21.61
CH_3CCH [?]	30.51	–	30.488
C_2N [?]	30.88	–	30.864

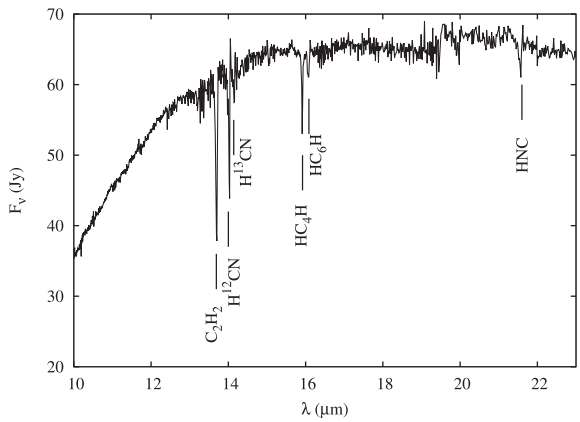

Figure 8. *Spitzer* spectrum showing absorption by small hydrocarbon molecules in Sakurai on 2005 April 15. Data de-reddened as described in the text.

8.1 HCN

8.1.1 The $^{12}C/^{13}C$ ratio

Using the strong $H^{12}CN$ feature at 14.03 μm in the *Spitzer* data, we find that the temperature is not particularly well constrained, with values lying between 350 and 450 K; this is a little lower than

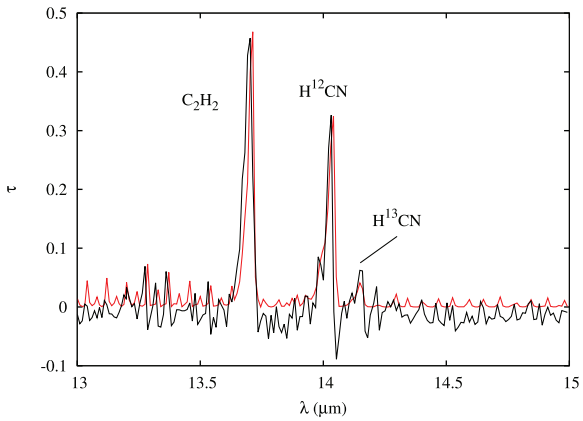

Figure 9. Fit of slab model as described in the text to $H^{12}CN$, $H^{13}CN$, and C_2H_2 for the 2005 April 15 *Spitzer* spectrum. Black curve, optical depth derived as described in the text; red curve, fit with parameters in Table 5.

that determined by Evans et al. (2006, ∼400–500 K). We attribute this difference to two factors: (a) the greater line width assumed here ($\simeq 10^{-3}\lambda$) compared to our previous work – leading to a lower temperature, and (b) the fact that, in this work, we use spectra extracted in a uniform way from the CASSIS archive, whereas in Evans et al. the data were reduced 'manually' using the SPICE (2005) software package.

Tafoya et al. (2017) detected the $J = 4 \rightarrow 3$ and $1 \rightarrow 0$ HCN rotational transitions in Sakurai, and deduced a rotational temperature 13 ± 1 K. They attributed the difference between their value and that deduced by Evans et al. (2006) to the fact that the gas they detected is observed over the entire circumstellar region, including cooler, more diffuse gas, whereas the *Spitzer* observations sampled hotter, denser, gas close to the dust shell. Further, the deduced gas temperature is greater than the corresponding temperature of the dust against which the features are seen in absorption. Clearly, the properties of the dust and gas in Sakurai's environment are far more complex than we have assumed here.

For our present purposes, we take a temperature of 400 K for the molecular gas, and the fit for 2005 April 15 is shown in Fig. 9. For each date, we have determined the corresponding column density for both $H^{12}CN$ and $H^{13}CN$ (see Table 5). The variation of the

Table 5. Column densities of HCN isotopologues and C_2H_2. Assumed gas temperature $T = 400$ K.

Date	MJD	Column density			$^{12}C/^{13}C^{(a)}$
		$H^{12}CN$	$H^{13}CN$	C_2H_2	
		(10^{17} cm^{-2})		(10^{18} cm^{-2})	
2005-04-15	53475.3	$1.78^{+0.22}_{-0.19}$	$0.20^{+0.05}_{-0.04}$	$1.15^{+0.30}_{-0.19}$	8.9 ± 0.3
2007-05-04	54224.9	$1.86^{+0.13}_{-0.20}$	$0.31^{+0.06}_{-0.04}$	–	5.9 ± 0.5
2007-10-15	54388	$1.91^{+0.23}_{-0.28}$	$0.35^{+0.15}_{-0.10}$	–	5.5 ± 0.7
2008-04-08	54564	$1.62^{+0.20}_{-0.21}$	$0.25^{+0.04}_{-0.04}$	$0.91^{+0.18}_{-0.19}$	6.5 ± 0.4
2008-10-18	54757.1	$1.88^{+0.30}_{-0.30}$	$0.36^{+0.07}_{-0.13}$	–	5.2 ± 0.6

Note. [(a)]From the HCN isotopologues.

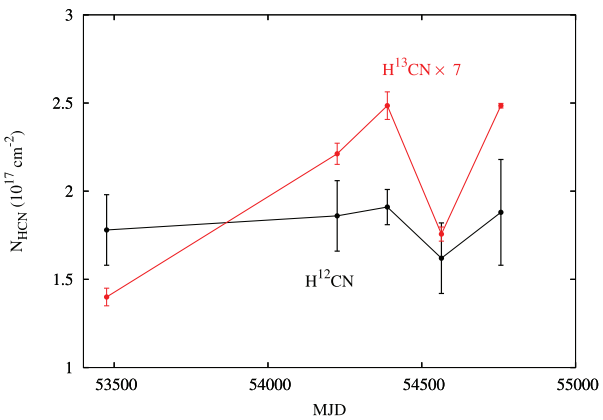

Figure 10. Variation of the HCN column densities with time as determined from the 14 μm feature in the *Spitzer* spectra. The $H^{13}CN$ data are multiplied by 7.

absorbing column density with time, for both isotopologues, is shown in Fig. 10.

For the simple spherically symmetric case, the column density N is related to the mass-loss rate $\dot{M}$ by

$$N = \frac{\dot{M}}{4\pi v \mu R_1}\left(1 - \frac{R_1}{vt}\right),$$

where v is the wind speed, μ is the mean molecular mass, and R_1 is the radius at the base of the wind. Taking the stellar luminosity L_* and temperature T_* from Hajduk et al. (2005) to estimate the stellar radius R_*, and assuming $R_1 \simeq R_*$, we get $R_1 \simeq 2.3 \times 10^9$ m. With a wind speed of 300 km s^{-1} (Tafoya et al. 2017) for $t \sim 20$ yr, the factor in brackets is close to unity, so that the column density is simply proportional to $\dot{M}$. There is no compelling evidence for any variation of the column density with time, suggesting that the mass-loss rate as measured by HCN was ∼ constant over the period from 2005 April to 2008 October. The mean column density in $H^{12}CN$ is 1.8×10^{17} cm^{-2}, a little larger than that found by Evans et al. (2006).

The ratio of the $H^{12}CN$ and $H^{13}CN$ column densities gives an estimate of the $^{12}C/^{13}C$ ratio. It is evident from Fig. 10 that – as reported by numerous authors (Pavlenko et al. 2004; Evans et al. 2006; Worters et al. 2009; Tafoya et al. 2017) – the $^{12}C/^{13}C$ ratio is very low. A mean of the values in Table 5 gives $^{12}C/^{13}C = 6.4 \pm 0.7$, about 1/14 of the solar value.

8.1.2 Implications

If the high abundance of ^{13}C derived above is a consequence of proton capture, the amount of ^{13}C produced depends on the amount of hydrogen initially present in the envelope. Effectively, each p gives rise to a ^{13}C, so the production of a mass of ^{13}C, M_{13}, requires the processing of $\sim M_{13}/13$ of hydrogen. Assuming that the relative numbers of ^{12}C and ^{13}C in the dust are the same as those in the gas phase, the dust mass of 2.0×10^{-5} M$_\odot$ implies a mass of ^{13}C in the dust of $\sim M_{\rm dust}/6.9 \simeq 2.9 \times 10^{-6}$ M$_\odot$. This requires the processing of $\sim 2.2 \times 10^{-7}$ M$_\odot$ of hydrogen, and an envelope mass of $\sim 3 \times 10^{-7}$ M$_\odot$ assuming solar abundances in the envelope.

As already noted (Section 2), we can rule out a progenitor with mass less than 1.25 M$_\odot$ for Sakurai. The envelope mass before the VLTP is given as a function of progenitor mass by Miller Bertolami (2016); his fig. 7 implies that the envelope on Sakurai's progenitor had mass at most $\sim 1.5 \times 10^{-4}$ M$_\odot$, which would likely have resulted in $\sim 2 \times 10^{-3}$ M$_\odot$ of ^{13}C. While some of the ^{13}C would have been further processed, the mass of ^{13}C alone seems consistent with the mass of carbon dust we have deduced.

8.2 C_2H_2

The isotopologues of acetylene display numerous ro-vibrational bands around 13 μm (see Cernicharo et al. 1999, especially their fig. 3, for details). We see these in absorption in two *Spitzer* IRS spectra, namely those obtained on 2005 April 15 (discussed in Evans et al. 2006) and 2008 April 8 (see Fig. 8); the *Spitzer* IRS spectra obtained on other dates are not of sufficient quality around 13 μm to reveal these features.

We have modelled these, for both $^{12}C_2H_2$ and $^{13}C^{12}CH_2$, using molecular data from the high-resolution transmission molecular absorption data base (HITRAN; Gamache, Hawkins & Rothman 1990; Rothman et al. 1998); the two isotopologues are not resolved in our data. We again assume a gas temperature of 400 K. We also assume that the relative abundance of the two isotopologues is determined simply by the $^{12}C/^{13}C$ ratio (6.4) determined from the HCN data, although this is likely to be an oversimplification.

The resulting column densities for C_2H_2 are given in Table 5, and the fit for 2005 April 15 is included in Fig. 9. There is no evidence that the C_2H_2 column density varied between 2005 April and 2008 October, and the mean column density is $1.0[\pm 0.3] \times 10^{18}$ cm^{-2}. This value is similar to that given in Evans et al. (2006).

8.3 Other features

In addition to HCN (Section 8.1), we report here the secure identification of the fundamental transition of hydrogen isocyanide (HNC) at 21.61 μm (Harris, Polyansky & Tennyson 2002). HNC is an isomer of HCN but lies high in energy (∼3700 eV) above HCN. The high abundance of HNC in interstellar clouds is generally attributed to the electron recombination with $HCNH^+$ (Graninger et al. 2014). Its presence in Sakurai could be an indication of ion–molecule chemistry.

In addition to the above molecular features, there are two weak features at 30.51 and 30.88 μm, which we tentatively identify with methyl acetylene (aka propyne; $CH_3{-}C{\equiv}CH$) and the radical C_2N, respectively (see Fig. 11). If correct, we believe that this is the first astrophysical observation of methyl acetylene in the IR. It has been observed in *young* ($\lesssim 10^3$ yr) PNe at millimetre wavelengths (see e.g. Schmidt & Ziurys 2019, and references therein), suggesting an origin in the Sakurai environment resulting from a recent mass-

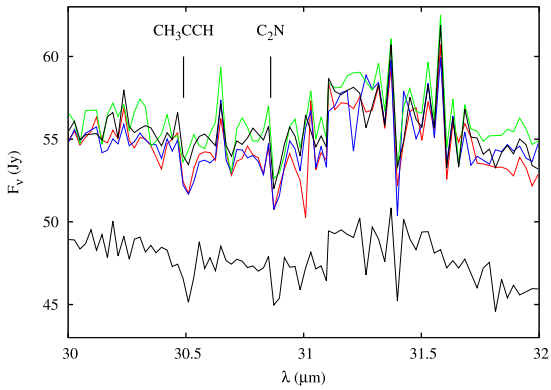

Figure 11. Absorption by CH_3CCH and C_2N in the spectral range 30–32 μm. Upper black: 2005-04-15; red: 2007-05-04; blue: 2007-10-15; green 2008-04-08; lower black: 2008-10-18. Data de-reddened as described in the text.

loss episode, such as that evidenced by the excess in Fig. 6. All subsequent *Spitzer* spectra display these features, which give us confidence in their reality; other apparent features either are present in only one spectrum, are present in only one spectral element, or are the result of mismatch in the flux scale between *Spitzer* grisms. However, the features in Table 4 and Fig. 8 do not appear in the *SOFIA* spectra, either because they have weakened to the extent that they are no longer detectable, or because they fall in spectral gaps between wavelength ranges covered by the *SOFIA* FORCAST grisms.

Methyl acetylene – in which one of the H atoms in acetylene is replaced by CH_3 – is commonly seen in dense interstellar molecular clouds, for which it is sometimes used as a thermometer (e.g. Askne et al. 1984; Kuiper et al. 1984). Hickson, Wakelam & Loison (2016) have argued that the formation of methyl acetylene is problematic in the gas phase (at least in molecular cloud and interstellar medium environments), and that it may most easily form via surface hydrogenation of C_3 on grain surfaces. Such a process must have occurred in the hydrogen-rich material ejected by Sakurai before its VLTP phase.

The formation of C_2N has been discussed – in the context of both interstellar and circumstellar environments – by Mebel & Kaiser (2002), who suggest that it might be formed via the route

$$C + HCN \longrightarrow C_2N + H.$$

Mebel and Kaiser note that this reaction is unlikely to proceed in the low temperatures in interstellar space but is likely to occur in warmer circumstellar environments. In view of the presence of HCN in Sakurai's environment, the presence of C_2N is not unexpected (although it was not detected in the archetypical carbon star IRC+10216 by Fuchs et al. 2004).

9 CONCLUSIONS

We have presented a 20-yr overview of the IR development of V4334 Sgr (Sakurai's object), highlighting the properties of the dust, and the evolution of the molecular absorption. Our principal findings and conclusions are as follows:

(i) The observable dust around Sakurai has cooled from ∼1200 K in 1998 to ∼180 K in 2016, and some 2×10^{-5} $M_\odot$ of amorphous carbon dust has formed between the commencement of the first dust phase in 1997 and the last *SOFIA* observation in 2016;

(ii) There is evidence, in the form of dust that is hotter than that ejected between 1998 and 2008, for a more recent dust ejection event, which commenced after 2008 October;

(iii) We have identified a number of small hydrocarbon and other molecules in absorption against the dust shell;

(iv) We find no significant variation in the column densities of HCN and C_2H_2 between 2005 April and 2008 October;

(v) We find possible evidence for absorption by nitrogenated HAC;

(vi) The $^{12}C/^{13}C$ ratio, based on the column densities of the HCN isotopologues, is found to be 6.4 ± 0.7, which is 14 times smaller than the solar value, and consistent with Sakurai being a VLTP object.

ACKNOWLEDGEMENTS

We thank the referee for their careful and thorough review of the first version of this paper, and for their constructive and helpful suggestions.

Based in part on observations made with the NASA/DLR SOFIA. SOFIA is jointly operated by the Universities Space Research Association, Inc. (USRA), under NASA contract NNA17BF53C, and the Deutsches SOFIA Institut (DSI) under DLR contract 50 OK 0901 to the University of Stuttgart.

This publication makes use of data products from the *WISE*, which is a joint project of the University of California, Los Angeles, and the Jet Propulsion Laboratory/California Institute of Technology, funded by the National Aeronautics and Space Administration.

It also makes use of data products from the 2MASS, which is a joint project of the University of Massachusetts and the Infrared Processing and Analysis Center/California Institute of Technology, funded by the National Aeronautics and Space Administration and the National Science Foundation.

Based on data products from VVV Survey observations made with the VISTA telescope at the ESO Paranal Observatory under programmes IDs 179.B-2002 and 198.B-2004. This research has made use of the services of the ESO Science Archive Facility.

RDG was supported by NASA and the United States Air Force. CEW acknowledges support from *SOFIA* and NASA. DPKB is supported by a CSIR Emeritus Scientist grant-in-aid, which is being hosted by the Physical Research Laboratory, Ahmedabad. TRG's research is supported by the Gemini Observatory, which is operated by the Association of Universities for Research in Astronomy, Inc., under a cooperative agreement with the NSF on behalf of the Gemini partnership: the National Science Foundation (United States), National Research Council (Canada), CONICYT (Chile), Ministerio de Ciencia, Tecnología e Innovación Productiva (Argentina), Ministério da Ciência, Tecnologia e Inovação (Brazil), and Korea Astronomy and Space Science Institute (Republic of Korea). PJS thanks the Leverhulme Trust for the award of a Leverhulme Emeritus Fellowship. SS acknowledges partial support from NASA and *HST* grants to ASU. TL acknowledges financial support from Grantová agentura České republiky (GAČR) (grant number 17-02337S). The Astronomical Institute Ondřejov is supported by the project RVO:67985815. This project has received funding from the European Union's Framework Programme for Research and Innovation Horizon 2020 (2014-2020) under the Marie Skłodowska-Curie Grant Agreement No. 823734.

REFERENCES

Aoki W., Tsuji T., Ohnaka K., 1999, A&A, 350, 945
Askne J., Hoglund B., Hjalmarson A., Irvine W. W., 1984, A&A, 130, 311
Asplund M., Gustafsson B., Lambert D. L., Kameswara Rao N., 1997, A&A, 321, L17
Asplund M., Lambert D. L., Kipper T., Pollacco D., Shetrone M. D., 1999, A&A, 343, 507
Ballik E. A., Ramsay D. A., 1963, ApJ, 137, 61
Blöcker T., 2001, Ap&SS, 275, 1
Bode M. F., Evans A., 1989, in Bode M. F., Evans A., eds, Classical Novae, 1st edn. Wiley, Chichester, UK, p. 163
Boyer M. L. et al., 2015a, ApJS, 216, 10
Boyer M. L. et al., 2015b, ApJ, 800, 51
Boyer M. L. et al., 2017, ApJ, 851, 152
Cernicharo J., Yamamura I., González-Alfonso E., de Jong T., Heras A., Escribano R., Ortigoso J., 1999, ApJ, 526, L41
Chesneau O. et al., 2009, A&A, 493, L17
Clarke M., Vacca W. D., Shuping R. Y., 2014, in Taylor A. R., Stil J. M., eds, ASP Conf. Ser. Vol. 495, Astronomical Data Analysis Software and Systems XXIV (ADASS XXIV). Astron. Soc. Pac., San Francisco, p. 355
Clayton G. C., Kerber F., Pirzkal N., de Marco O., Crowther P. A., Fedrow J. M., 2006, ApJ, 646, L69
Clayton G. C. et al., 2013, ApJ, 771, 130
Cutri R. M. et al., 2012, Explanatory Supplement to the WISE All-Sky Data Release Products. available at: http://wise2.ipac.caltech.edu/docs/release/ allsky/expsup/index.html
Dürbeck H. W., 2002, Ap&SS, 279, 5
Dürbeck H. W., Benetti S., 1996, ApJ, 468, L111
Evans A., 1993, The Dusty Universe. Wiley Praxis, Chichester, UK
Evans A. et al., 2002a, MNRAS, 332, L69
Evans A., Geballe T. R., Smalley B., Tyne V. H., Eyres S. P. S., 2002b, A&A, 394, 971
Evans A., Geballe T. R., Tyne V. H., Pollacco D., Eyres S. P. S., Smalley B., 2004, MNRAS, 353, L41
Evans A. et al., 2006, MNRAS, 373, L75
Evans A. et al., 2017, MNRAS, 466, 4221
Eyres S. P. S., Richards A. M. S., Evans A., Bode M. F., 1998a, MNRAS, 297, 905
Eyres S. P. S., Evans A., Geballe T. R., Salama A., Smalley B., 1998b, MNRAS, 298, L37
Fuchs G. W., Fuchs U., Giesen T. F., Wyrowski F., 2004, A&A, 426, 517
Gaia Collaboration, 2018, A&A, 616, A1
Gamache R. R., Hawkins R. L.,Rothman L. S. , 1990, J. Mol. Spectrosc., 142, 205
García-Hernández D. A., Kameswara Rao N., Lambert D. L., 2013, ApJ, 773, 107
Geballe T. R., Evans A., Smalley B., Tyne V. H., Eyres S. P. S., 2002, Ap&SS, 279, 39
Gehrz R. D., Woodward C. E., Temim T., Lyke J. E., Mason C. G., 2005, ApJ, 623, 1105
Gehrz R. D. et al., 2007, Rev. Sci. Instrum., 78, 011302
Gehrz R. D. et al., 2015, ApJ, 812, 132
Gehrz R. D. et al., 2018, ApJ, 858, 78
Goldman S. R., 2019, ApJ, 877, 49
Gonzalez O. A., Rejkuba M., Zoccali M., Valenti E., Minniti D., Schultheis M., Tobar R., Chen B., 2012, A&A, 543, A13
Graninger D. M., Herbst E., Öberg K. I., Vasyunin A. I., 2014, ApJ, 787, 76
Green G. M. et al., 2018, MNRAS, 478, 651
Grishko V. I., Duley W. W., 2002, ApJ, 568, 448
Hajduk M. et al., 2005, Science, 308, 231
Harris G. J., Polyansky O. L., Tennyson J., 2002, Spectrochim. Acta A, 58, 673
Herter T. L. et al., 2012, ApJ, 749, L18
Herter T. L. et al., 2013, PASP, 125, 1393
Herwig F., 2001, ApJ, 554, L71
Herwig F., 2005, ARA&A, 43, 435
Herwig F., Pignatari M., Woodward P. R., Porter D. H., Rockefeller G., Fryer C. L., Bennett M., Hirschi R., 2011, ApJ, 727, 89
Hickson K. M., Wakelam V., Loison J.-C., 2016, Mol. Astrophys., 3, 1
Hinkle K. H., Joyce R. R., 2014, ApJ, 785, 146
Hinkle K. H., Joyce R. R., 2015, in Kerschbaum F., Wing R. F., Hron J., eds, ASP Conf. Ser. Vol. 497, Why Galaxies Care about AGB Stars III. Astron. Soc. Pac., San Francisco, p. 303
Hinkle K. H., Lebzelter T., Joyce R. R., Ridgway S., Close L., Hron J., Andre K., 2008, A&A, 479, 817
Hinkle K. H., Joyce R. R., Matheson T., 2017, Am. Astron. Soc. Meeting, #229, 154.11
Houck J. R. et al., 2004, ApJS, 154, 18
Iben I., 1982, ApJ, 260, 821
Iben I., Renzini A., 1983, ARA&A, 21, 271
Ivezić Ž., Elitzur M., 1995, ApJ, 445, 415
Jeffery C. S., Schönberner D., 2006, A&A, 459, 885
Jones A. P., Köhler M., Ysard N., Bocchio M., Verstraete L., 2017, A&A, 602, A46
Kerber F., Gratl H., Kimeswenger S., Weinberger R., Roth M., Duffee B., 1997, in Habing H. J., Lamers H. J. G. L. M., eds, Proc. IAU Symp. 180, Planetary Nebulae. Kluwer Acad. Publishers, Dordrecht, p. 390
Kimeswenger S., 2002, Ap&SS, 279, 79
Kuiper T. B. H., Rodriguez Kuiper E. N., Dickinson D. F., Turner B. E., Zuckerman B., 1984, ApJ, 276, 211
Lawlor T. M., MacDonald F., 2003, ApJ, 583, 913
Lebouteiller V., Barry D. J., Spoon H. W. W., Bernard-Salas J., Sloan G. C., Houck J. R., Weedman D. W., 2011, ApJS, 196, 8
Lebouteiller V., Barry D. J., Goes C., Sloan G. C., Spoon H. W. W., Weedman D. W., Bernard-Salas J., Houck J. R., 2015, ApJS, 218, 21
Lodders K., Palme H., Gail H. P., 2009, in Trümper J. E., ed., Landolt-Börnstein, Vol. VI/4B, Chap. 4.4. Springer-Verlag, Berlin, p. 560
Mainzer A. et al., 2014, ApJ, 792, 30
Marshall D. J., Robin A. C., Reyle C.,Schultheis M., Picaud S. , 2006, A&A, 453, 635
Mebel A. M., Kaiser R. I., 2002, ApJ, 564, 787
Miller Bertolami M. M., 2016, A&A, 588, A25
Nakano S., Sakurai Y., Kojima T., 1996, IAU Circ., 6322, #1
Pavlenko Y. V., Geballe T. R., 2002, A&A, 390, 621
Pavlenko Y. V., Geballe T. R., Evans A., Smalley B., Eyres S. P. S., Tyne V. H., Yakovina L. A., 2004, A&A, 417, L39
Pollacco D., 1999, MNRAS, 304, 127
Rothman L. S. et al., 1998, J. Quant. Spectrosc. Radiat. Transfer, 60, 665
Saito R. K. et al., 2012, A&A, 537, A107
Schmidt D. R., Ziurys L. M., 2019, ApJ, 881, L38
Skrutskie M. F. et al., 2006, AJ, 131, 1163
Sloan G. C. et al., 2009, Science, 323, 353
SPICE User's Guide, Version 1.1, 2005. (Available at: https://irsa.ipac.caltech.edu/data/SPITZER/docs/dataanalysistools/tools/spice/ (accessed date 2006)
Swan W., 1857, Trans. R. Soc. Edinburgh, 21, 411
Tafoya D. et al., 2017, A&A, 600, A23
Temi P. et al., 2014, ApJS, 212, 24
Tyne V. H., Eyres S. P. S., Geballe T. R., Evans A., Smalley B., Dürbeck H. W., Asplund M., 2000, MNRAS, 315, 595
Tyne V. H., Evans A., Geballe T. R., Eyres S. P. S., Smalley B., Dürbeck H. W., 2002, MNRAS, 334, 875
Van de Steene G. C., van Hoof P. A. M., Kimeswenger S., ZIjlstra A. A., Avison A., Guzman-Ramirez L., Hajduk M., Herwig F., 2016, in Liu X., Stanghellini L., Karakas A., eds, Proc. IAU Symp. 323, Planetary Nebulae: Multi-Wavelength Probes of Stellar and Galactic Evolution. Cambridge Univ. Press, Cambridge, UK, p. 380
van Hoof P. A. M. et al., 2007, A&A, 471, L9

van Hoof P. A. M., Kimeswenger S., Van de Steene G. C., Zijlstra A. A., Hajduk M., Herwig F., 2015, in Dufour P., Bergeron P., Fontaine G., eds, ASP Conf. Ser. Vol. 493, The Very Fast Evolution of the VLTP Object V4334 Sgr. Astron. Soc. Pac., San Francisco, p. 95
Werner M. W. et al., 2004, ApJS, 154, 1
Worters H. L., Rushton M. T., Eyres S. P. S., Geballe T. R., Evans A., 2009, MNRAS, 393, 108
Wright E. L. et al., 2010, AJ, 140, 1868
Young E. T. et al., 2012, ApJ, 749, L17

APPENDIX A: THE OBSERVED FLUX

For a blackbody emitter having temperature T and flux density

$$f_\lambda = \frac{F}{\lambda^5}\,\frac{1}{\exp(B/\lambda)-1},$$

where F and $B = hc/kT$ are the constants, it is trivially shown that the wavelength $\lambda_{\rm m}$ at which $[\lambda f_\lambda]$ is a maximum is $\lambda_{\rm m} = B/\alpha$; here, α ($\simeq$3.9207...) is the solution of the transcendental equation

$$4\,(1-e^{-\alpha}) = \alpha.$$

Thus,

$$[\lambda f_\lambda]_{\rm max} = F\left(\frac{\alpha}{B}\right)^4 \frac{1}{{\rm e}^{\alpha}-1},$$

as used in Section 6.

Furthermore, the total observed flux f for a blackbody source of radius R and distance D, in the absence of an intervening medium, is

$$f = \int_0^\infty f_\lambda {\rm d}\lambda = \frac{\pi R^2}{D^2}\,\frac{\sigma T^4}{\pi}. \tag{A1}$$

For a blackbody, f is related to $[\lambda f_\lambda]_{\rm max}$ by

$$f = \frac{\pi^4}{15}[\lambda f_\lambda]_{\rm max}\left(\frac{e^\alpha-1}{\alpha^4}\right) \simeq 1.359\ldots[\lambda f_\lambda]_{\rm max}, \tag{A2}$$

where σ is the Stefan–Boltzmann constant, as used in Section 6.

Finally, the 'blackbody angular diameter' $\theta_{\rm BB}$ is given by

$$\theta_{\rm BB} = \frac{2R}{D} = \frac{2.331}{\sigma^{1/2}T^2}\,[\lambda f_\lambda]_{\rm max}^{1/2}$$

so that

$$\theta_{\rm BB} = 2.02\times 10^9\,[\lambda f_\lambda]_{\rm max}^{1/2}\,T^{-2},$$

where $\theta_{\rm BB}$ is in arcsec and $[\lambda f_\lambda]_{\rm max}$ is in W m^{-2}.

This paper has been typeset from a TEX/LATEX file prepared by the author.